frontiers in Materials

ORIGINAL RESEARCH
published: 18 March 2020
doi: 10.3389/fmats.2020.00030

Three-Dimensional Graphene-Decorated Copper-Phosphide (Cu_3P@3DG) Heterostructure as an Effective Electrode for a Supercapacitor

Subodh Kumar[1†], S. K. Tarik Aziz[1†], Sushil Kumar[2†], Sk Riyajuddin[2], Gili Yaniv[3], Louisa Meshi[3], Gilbert D. Nessim[1]* and Kaushik Ghosh[2]**

[1] Department of Chemistry, Bar-Ilan Institute for Nanotechnology and Advanced Materials, Bar-Ilan University, Ramat Gan, Israel, [2] Institute of Nano Science & Technology, Mohali, India, [3] Department of Materials Engineering, Ben-Gurion University of the Negev, Beer-Sheva, Israel

OPEN ACCESS

Edited by:
Federico Cesano,
University of Turin, Italy

Reviewed by:
David Aradilla,
Commissariat à l'Energie Atomique et aux Energies Alternatives (CEA), France
Shuling Liu,
Shaanxi University of Science and Technology, China

***Correspondence:**
Louisa Meshi
lmeshi.lm@gmail.com
Gilbert D. Nessim
Gilbert.Nessim@biu.ac.il
Kaushik Ghosh
kaushik@inst.ac.in

† These authors have contributed equally to this work

Specialty section:
This article was submitted to Energy Materials, a section of the journal Frontiers in Materials

Received: 28 October 2019
Accepted: 28 January 2020
Published: 18 March 2020

Citation:
Kumar S, Aziz SKT, Kumar S, Riyajuddin S, Yaniv G, Meshi L, Nessim GD and Ghosh K (2020) Three-Dimensional Graphene-Decorated Copper-Phosphide (Cu_3P@3DG) Heterostructure as an Effective Electrode for a Supercapacitor. Front. Mater. 7:30. doi: 10.3389/fmats.2020.00030

Transition metal phosphides already emerged with great interest due to their energy storage capacitance, superior metalloid characteristics, and decent electrical conductivity. To achieve a commercially viable outcome, these electrodes are fabricated with interconnected carbonaceous materials. Herein, we have synthesized hexagonal copper phosphide (Cu_3P) platelets using chemical vapor deposition (CVD) and integrated it with highly conducting three-dimensional graphene (3DG), leading to a nanohybrid (Cu_3P@3DG) as a coulombic efficient supercapacitor. This nanohybrid has exhibited a specific capacitance (C_{sp}) of 1,095.85 F/g at 10 mV/s scan rate along with a cycling stability of 95% capacitive retention after 3,000 cycles at a current density of 8.97 A/g. The C_{sp} is almost four times higher and the stability is 1.2 times higher compared to the bare Cu_3P platelets. We have fabricated an asymmetric supercapacitor (ASC) using Cu_3P@3DG on graphite as cathode and activated carbon (AC) on graphite as anode (Cu_3P@3DG//AC) that has shown high specific capacity (108.78 F/g), energy density (8.23 Wh/kg), and power density (439.6 W/kg). Moreover, this ASC has exhibited an excellent life cycle (5,500 consecutive charge–discharge with 96% coulombic efficiency). Therefore, the proposed all-solid-state hybrid device can be considered as a route for next-generation high-performing energy storage devices.

Keywords: hexagonal copper phosphide platelets, chemical vapor deposition, red phosphorus, three-dimensional graphene (3DG), energy storage devices

INTRODUCTION

The relentless increase in energy demand and parallel steady reduction of fossil fuels drive the scientific and industrial need to develop renewable energy along with faster and compatible energy storage devices (Li et al., 2015, 2017; Zhang et al., 2019). Supercapacitors represent essential components that can bridge between stereotype capacitors and rechargeable batteries in terms of power and energy densities with a long cycle life (Wang et al., 2018; Cao et al., 2019;

Chen et al., 2019). In recent times, the synthesis of materials having semiconducting, metalloid, and energy storage properties has emerged at the forefront of research activities (Augustyn et al., 2014; López-Ortega et al., 2015; Sivula and Van De Krol, 2016). The transition metal phosphides are a fascinating class of materials because of their wide range of properties depending on their size and shape (Barry et al., 2008; Shao et al., 2017; Aziz and Islam, 2018). Metal phosphides have been tested and found to be active catalysts with their potential applications in electro-catalysis and photo-catalysis. In the last few years, several phosphides of nickel, cobalt, iron, molybdenum, tungsten, copper, and many more with different morphologies and crystallinity have been synthesized using different methods including phosphorization, electrodeposition, and ball milling (Brock et al., 2004; Henkes et al., 2007; Barry et al., 2008; Brock and Senevirathne, 2008; Wang et al., 2010). Metal phosphides with controlled nanostructures and elemental compositions have been designed and reported to provide significant enhancement in electrochemical activity (Wang et al., 2015a; Chen et al., 2016; Seo et al., 2016; Wu H. et al., 2016). Also, metal phosphides have metalloid properties and exhibit high specific capacitances (C_{sp}) and high volumetric and gravimetric capacities with lower intercalation potentials compared to commercial carbonaceous materials. Thus, they have attracted extensive interest to design novel electrode materials for supercapacitors rather than lithium-ion batteries (Li et al., 2017). Although transition metal hydroxides, metal oxides, and polymers (conducting) are commonly used electrode materials for lithium-ion batteries and pseudo-capacitors (Wang et al., 2015a,c; Zhu et al., 2015; Wu J. et al., 2016), however, these materials are kinetically slow for the fast electron transport and that invariably required for high-power density with moderate energy density (Li et al., 2017).

Copper phosphide (Cu_3P) is an air-stable, low-cost, environment-friendly material that exhibits high volumetric as well as comparable gravimetric capacity to that of graphite (Pfeiffer et al., 2004). Cu_3P have also been explored widely in the field of photo/electro-catalytic water splitting (Sun et al., 2015; Wei et al., 2016; Han et al., 2017; Hao et al., 2016). Recently, this material has been introduced in the energy storage sector to bridge the gap between electric double-layer capacitor (EDLC) and batteries (Chen et al., 2017; Zhang et al., 2019). It has been proved that the electrochemical activity of a material is strongly affected by its size, structure, and chemical composition. Cu_3P with different morphology and crystallinity have been synthesized and investigated for energy storage devices showing an improvement in electrochemical activities (Liu et al., 2012, 2016; Fan et al., 2016).

Carbonaceous matrices [e.g., graphene, carbon natotube (CNT), graphite, etc.] are simultaneously proved to be a promising choice of electrode material due to its high conductivity, large surface area, flexibility, and transparency which drags its attention toward large-scale applications in energy storage devices. Among various carbonaceous materials, three-dimensional graphene (3DG) is the promising choice as a backbone for electroactive materials for supercapacitor due to the random orientation of graphene flakes in three dimensions leading to the formation of micro/mesoporous structures (Mukherjee and Austeria, 2016; Singh et al., 2017; Xue et al., 2018). The 3DG provides high conductive channels for ion and electron transfer in charging–discharging cycles leading to a prominent improvement in overall capacitive performance of electroactive materials. Also, 3DG effectively minimizes the unwanted agglomeration of metal nanoparticles, thereby enhancing the chemical stability of the electroactive materials. In compliance to develop a novel approach for the synthesis of new hybrid materials (Kumar et al., 2017; Itzhak et al., 2018) herein, we report a facile, industrially scalable and easy method to produce a high yield of hexagonal Cu_3P by solid-state reaction at low temperature followed by the formation of nano-hybrid with 3DG matrix on graphite substrate. This nano-hybrid has demonstrated significantly high electrochemical performance at an optimized Cu_3P:3DG ratio with a tremendous C_{sp} of 1,095.85 F/g at a scan rate of 10 mV/s. The asymmetric device of Cu_3P@3DG electrode (positive) and activated carbon (AC) (negative electrodes) on graphite substrate reveals worthy performance in power densities, cycling stability, and excellent capacitive retention.

EXPERIMENTAL SECTION

Materials

The copper foil was purchased from Alfa-Aesar. Red phosphorus was purchased from Sigma Aldrich and was used without any further purification. A compressed cylinder tank of argon gas was procured from Gas Technologies with a purity of 99.999%. An atmospheric-pressure three-zone chemical vapor deposition (CVD) furnace, fitted with a quartz tube with an internal diameter of 22 mm, was used for the synthesis. The built-in furnace thermocouples measured the furnace temperatures, and the flow of argon was maintained using electronic mass flow controllers (MKS P4B with digital mass flows control unit model 247D). Graphite powder, H_2SO_4, ortho-phosphoric acid, potassium permanganate, H_2O_2 (30%), HCl, polyvinyl alcohol, potassium hydroxide, graphite sheet, nafion, and AC were purchased from TCI Chemicals India. Glassy carbon electrode was purchased from Sinsil International Pvt. Ltd.

Synthesis of Hexagonal Copper Phosphide Platelets

Usual techniques to synthesize transition metal phosphide is *via* plasma-enhanced CVD (PECVD) using PH_3 plasma (Liang et al., 2017) or multistep hydrothermal techniques (Zhou et al., 2015; Ding et al., 2019) *via* metal oxide/hydroxide intermediate followed by thermal annealing. Using the PECVD approach restricts the phosphorization on the material surface rather than bulk conversion. On the other hand, hydrothermal growth may lead to polycrystalline phosphides and oxide intermediates that are difficult to avoid, which may possibly be responsible for degrading the electrochemical performance.

CVD has been shown as a one-step process where hexagonal Cu_3P can be synthesized at an optimized temperature (Wei et al., 2016; Riyajuddin et al., 2019). In a typical experimental

procedure, 50 mg of red phosphorus is kept in a quartz boat and then covered with a 0.25-mm-thick copper foil (the native oxide layer on Cu-foil is removed by sonication with 4 M HCl for 20 min and washed with distilled water and isopropanol and then dried) as shown in **Supplementary Figure S1**. Initially, there is no direct physical contact between the red phosphorus and the copper foil, which is positioned above the red phosphorus-containing boat. This quartz boat is inserted in the quartz tube and positioned at the center of the furnace and heated at 450°C for 5 min under a flow of Ar (25 sccm) at an ambient pressure condition. In this process, phosphorus particles sublimate which are diffused into the copper and reacted with it to nucleate Cu_3P crystallites and then grow into hexagonal platelets. A layer of dark shining gray color is observed on the surface of the copper foil exposed to the red phosphorus environment.

The synthesis of Cu_3P experiments is performed by using the "fast-heat" technique in which the samples are initially positioned outside the heated zone of the furnace with a fan blowing on the exposed quartz tube surface to keep the sample at room temperature (Itzhak et al., 2018; Kumar et al., 2018). Once the set temperatures of furnaces have reached a stable value, then the quartz tube is shifted to position the sample in the growth zone to start the phosphorization process. Using this technique, the sample is placed immediately to the required growth temperature and avoided exposure during the ramping steps.

Synthesis of the Three-Dimensional Graphene Matrix

The modified hydrothermal reduction method has been used for the synthesis of 3DG on top of the graphite sheet as reported in our earlier work (Singh et al., 2017). Briefly, a piece of graphite sheet is dipped into 2 mg/ml aqueous dispersion of graphene oxide. This aqueous dispersed solution of the graphene along with graphite sheets is freeze-dried at −20°C for 12 h. After that, the solution temperature is allowed to reach room temperature followed by the addition of 0.6 ml of 2 M ascorbic acid to the graphene oxide aqueous dispersion, and the mixture is sealed in a Teflon-lined autoclave and heated in an oven at 120°C for 6 h. The as-grown material is thoroughly dried in a vacuum for the formation of a porous 3DG-coated graphite electrode.

Assembly of a Solid-State Asymmetric Supercapacitor Device

The ASC devices are assembled by utilizing the Cu_3P@3DG on graphite electrode as positive electrodes and AC on graphite as negative electrodes with polyvinyl alcohol (PVA)/KOH as gel electrolyte. The KOH/PVA gel electrolyte is prepared by mixing 5 g KOH and 4 g PVA in 50 ml distilled water with vigorous stirring at 90°C until the mixture solution becomes clear to form a semi gel state. Then, the prepared homogeneous 1 ml of each Cu_3P solution [∼0.3, 0.6, 0.91, 1.2, 1.5 mg/ml in Isopropyl alcohol (IPA)] is drop casted on top of 3DG-graphite electrodes (1 cm^2 × 1 cm^2) homogeneously and dried. Each electrode is covered with ∼1.1 mg of 3DG matrix. After that, the gel electrolyte is sandwiched between Cu_3P@3DG and AC electrodes, and the solid-state device is assembled successfully by moderate pressing to remove excess gel electrolytes and dried overnight. The active device area is 1 cm^2 × 1 cm^2, where longitudinally extended graphites are being used for making the connection for electrochemical measurement.

RESULTS AND DISCUSSION

In this work, hexagonal platelets were directly grown on copper foil by thermal annealing using a CVD system. A known amount of red phosphorus was kept in a quartz boat and covered with copper foil as shown in **Supplementary Figure S1**. Red phosphorus and copper foil were then heated at 450°C for 5 min under argon flow. A dark shiny gray color layer that formed on the red phosphorus-exposed side of the copper foil indicated the successful growth of Cu_3P. To investigate the effect of temperature on the morphology of Cu_3P on copper foil, the same experiment was repeated at 350, 450, 600, and 800°C. When the temperature was increased to 600°C, the material started losing its hexagonal morphology by condensing hexagonal platelets together. Upon further enhancement of the temperature up to 800°C, the entire hexagonal morphology was lost. On the other hand, lowering the temperature to 350°C, the hexagonal platelets did not nucleate, as shown in **Supplementary Figure S2**. These results confirmed that a specific temperature (450°C) was required for the growth of hexagonal platelets. HRSEM analysis of the synthesized Cu_3P revealed stacked platelets of hexagonal morphology with a lateral dimension in the range of micrometers and a thickness of a few nanometers, as shown in **Figure 1A**. HRSEM images and the corresponding elemental mapping patterns of Cu and P had demonstrated that the Cu and P elements were uniformly distributed on the hexagonal platelets (**Supplementary Figures S3c,d** in ESI). Transmission electron microscopy (TEM) analysis was performed for in-depth characterization. A low-magnification image, shown in **Figure 1B**, illustrated the nature of the hexagonal platelets. It was found that they consist of domains, although TEM sample preparation might influence the agglomeration (**Supplementary Figure S4**). The electron diffraction pattern taken from the agglomerate portion (**Supplementary Figure S4a**) was successfully indexed in terms of the hexagonal structure of the Cu_3P. It should be noted that the rings on the polycrystalline electron diffraction pattern indicated a large misorientation between the domains in the agglomerate. Using HRTEM, we studied small nano-sized domains constituting the agglomerate and did selected area electron diffraction (SAED), shown in **Figures 1C–D**. The SAED pattern was taken along [0001] orientation of one domain, and the corresponding HRTEM image is shown in **Supplementary Figure S4b**. In **Supplementary Figures S4b,c**, HRTEM image and SAED patterns were taken along [101 $^{-}$0] orientation of the domain fitting the atomic structure of Cu_3P, as reported by Olofsson (1972).

The phase content of the synthesized material was studied using X-ray diffraction (XRD) (**Figure 1E**). The XRD pattern exhibited strong, sharp peaks which were indexed in terms of hexagonal structure (P63cm) of the Cu_3P (JCPDS card no.

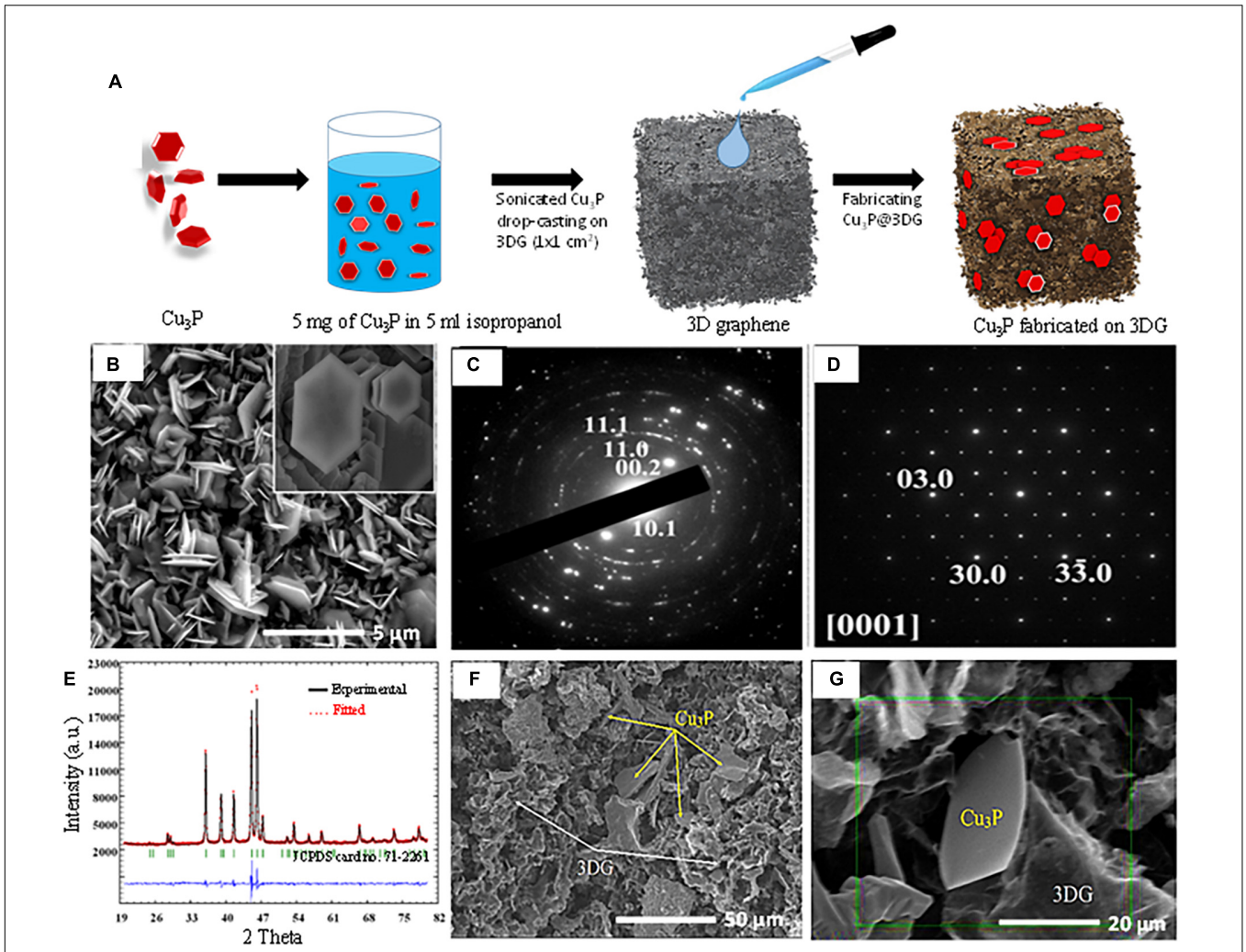

FIGURE 1 | (A) Schematic representation of synthesis of three-dimensional graphene-decorated copper phosphide (Cu_3P@3DG). **(B)** After synthesized Cu_3P pallets, HR-SEM images of hexagonal Cu_3P (hexagonal flake is shown inset). **(C)** Electron diffraction pattern taken from the agglomerate was indexed in terms of the hexagonal structure of the Cu_3P. **(D)** Selected area electron diffraction (SAED) patterns taken along [0001] orientation of one domain. **(E)** Rietveld refinement of Cu_3P: observed X-ray profile (open red circles), calculated profile (solid black line), and the difference between them (blue line on the bottom). Vertical bars refer to the calculated peak (JCPDS #71-2261). **(F)** Hybrid structure of hexagonal Cu_3P platelets on the three-dimensional (3DG) template. **(G)** HR-SEM represents the hybrid Cu_3P@3DG structure.

71-2261) (Hou et al., 2016). Rietveld refinement resulted in reliability factors: R_p = 2.3%, R_{wp} = 3.27%, R_{Bragg} = 1.05%, and R_{exp} = 1.73%. These low-reliability values excluded the possibility of the presence of impurities. It should be noted that atomic positions, occupancies, and thermal displacement parameters of the Cu_3P structure were not refined here, and the background was treated as linear. Lattice parameters were refined as a = 0.69673(1) nm and c = 0.71484(8) nm. The dependence of stoichiometry, temperature, and lattice parameters of the Cu_3P structure was discussed in the earlier report (Olofsson, 1972). Since the refined lattice parameters (i.e., a = 0.697, c = 0.7145 nm) were fitted well with reported parameters (Olofsson, 1972), thus the synthesized material was stoichiometric (or closely stoichiometric) as Cu_3P. To the best of our understanding, Rietveld refinement result of the as-synthesized sample was known to be the significant evidence for the formation of stoichiometric Cu_3P rather than the energy-dispersive X-ray spectroscopy (EDS) shown in **Supplementary Figure S3**. The presence of elements could be found in the EDS analysis. However, it was hard to estimate the stoichiometry *via* EDS since a large difference in atomic numbers of the constituents did not allow accurate standard in the EDS analysis. **Figure 1F** showed the formation of a hybrid porous structure made of hexagonal Cu_3P platelets along with 3DG. Careful observation indicated that the hexagonal Cu_3P platelets (shown by yellow arrows) were randomly scattered on the porous foamy 3DG architecture (shown by white arrows). A close-up view of these hybrid structures, shown in **Figure 1G**, revealed a single flake of Cu_3P trapped inside the 3DG matrix where a detailed EDS elemental mapping was performed to identify the

distribution of Cu, P, and C elements, respectively, shown in **Supplementary Figure S5**.

The X-ray photoelectron spectroscopy (XPS) analysis of Cu_3P elucidated the oxidation states and chemical interaction between Cu and red phosphorus (**Supplementary Figure S6**). The Cu, P, O, and C peaks appeared in the survey scan (shown in **Supplementary Figure S6a**). The presence of O1s peak indicated the superficial oxidation of Cu_3P, while the carbon peak was due to the background. The high-resolution XPS spectrum of Cu 2p (**Supplementary Figure S6b**) exhibited two peaks at 932.4 and 934.8 eV, which were attributed to phosphorized copper (Cu–P) and oxidized copper (Cu–O), respectively (Lin et al., 2016; Jin et al., 2017). **Supplementary Figure S6c** showed double peaks in the phosphorus region. The peak at 133.6 eV was due to the oxidized phosphorus in the form of phosphate (Li et al., 2016), and 129.7 eV was the binding energy of P in Cu_3P, which was lower than that of the binding energy of red phosphorus (130.2 eV), suggesting the conversion of copper to Cu_3P (Pfeiffer et al., 2005). The presence of Cu–O and POx was probably due to oxide layer formation on the surface of Cu_3P in ambient conditions.

To evaluate the as-grown nanomaterial as the promising electrode material, cyclic voltammetry (CV), galvanostatic charge–discharge (GCD), and electrochemical impendance spectroscopy (EIS) measurements were made to investigate the supercapacitive performance. The electrochemical window for CV and GCD measurements was kept in −0.5 to +0.5 V shown in **Figures 2A,B**. **Figure 2A** showed CV of the Cu_3P nanoplatelets under a three-electrode system in 1 M Na_2SO_4 electrolyte at a different scan rate from 10 to 200 mV/s. The broad shape of the asymmetric CV curves observed for Cu_3P nanoplatelets in the whole potential window indicated the presence of faradic behavior leading to pseudocapacitance along with electric double-layer capacitance (EDLC) existing simultaneously.

The appearance of two humps in between −0.5 and +0.5 V corresponding to cathodic and anodic maxima indicated that the Cu_3P platelets possess pseudocapacitive properties. These redox reactions attributed to the transition between metallic Cu(0) and Cu(I) species at an applied potential approximately −0.3 V vs. Ag/AgCl. While at the higher potential of 0.05 V vs. Ag/AgCl, the oxidation of Cu_3P platelets to Cu(II) species was observed due to aqueous interaction (**Figure 2A**). Further, the broad anodic peak nearly at 0.3 V could be attributed to the formation of a hydrous oxide of copper which originated from the hydrated cupric oxide (Jayalakshmi and Balasubramanian, 2008), and the corresponding chemical reaction was shown in equation (3). Here, the potential window had been fixed to 0.5 V to avoid the formation of Cu(III) species. So far, the identification of intermediate species was hard to find due to the chemical transformation of Cu_3P electrodes under electrochemical analysis, and the reaction mechanism was entirely unknown which required further detailed investigation. However, based on the available relevant literature, a possible

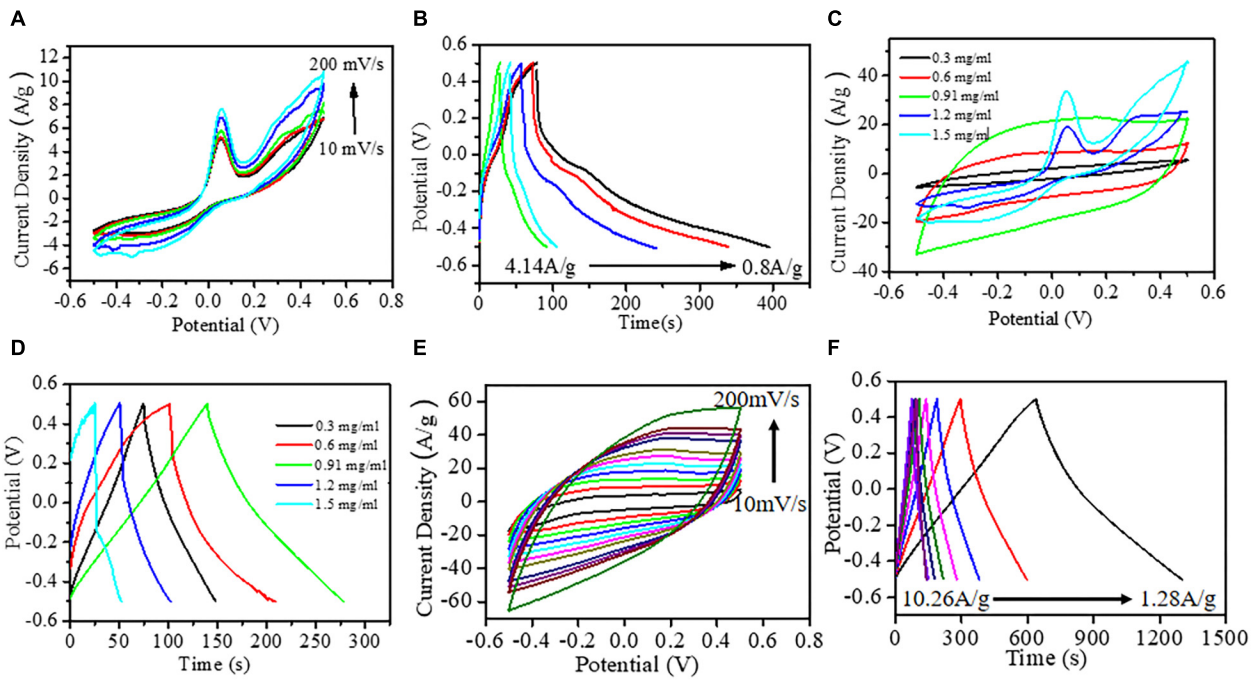

FIGURE 2 | Electrochemical characterization. **(A)** Typical cyclic voltammetry (CV) curves of hexagonal copper phosphide (Cu_3P) platelets on glassy carbon electrode at different scan rates (10, 50, 100, 150, and 200 mV/s). **(B)** Galvanostatic charge–discharge curves of Cu_3P platelets at various current densities. **(C)** CV curves at 50 mV/s scan rates for different rational compositions (0.3, 0.6, 0.91, 1.2, and 1.5 mg/ml) of Cu_3P on 3DG-graphite electrode. **(D)** Corresponding galvanostatic charge–discharge curves at 5.13 A/g current density. **(E)** Typical CV curves at different scan rates with the best weight ratio of 0.91 mg/ml of Cu_3P on graphite electrode (10–200 mV/s). **(F)** Corresponding galvanostatic charge–discharge curves at various current densities.

reaction mechanism had been proposed in the following equations (Poli et al., 2016; Chen et al., 2017).

$$Cu(I)_3P + xNa^+ + xe^- \rightarrow Na_x\{Cu(0)_xCu(I)_{3-x}\}P \quad (1)$$

$$Cu(I)_3P + H_2O \rightarrow Cu(II)_yO_yCu(I)_{3-y}P + 2_yH^+ + 2ye^- \quad (2)$$

$$CuO + H_2O \rightarrow Cu(OH)_2 \quad (3)$$

This mechanism could be attributed to redox reactions on the surface of Cu_3P platelets. Pfeiffer et al. (2004) had explained that all the elements of the first transition metal series have partially filled 3d shells, except copper and zinc. Nonetheless, only the copper has a complete 3d shell and a single 4 s electron. Hence, copper was the only element in the series to have M^{+1} state with filled D-orbital in Cu_3P platelets. The enhanced electrochemical performance might be attributed to the fact that the hexagonal Cu_3P platelets were composed of many small particles, which had significantly increased the specific surface area and provided more reaction sites on the surface evident from the SEM image shown in **Figures 1F,G**.

To further improve the Cu_3P electrode performance, we had designed a hybrid electrode with 3DG. The homogeneous distribution of Cu and P in hexagonal Cu_3P flake and carbon in the foamy graphitic matrix had confirmed the formation of Cu_3P@3DG hybrid network (shown in **Supplementary Figure S5**). For the development of effective electrode material, it was highly required to estimate the electrical conductivity of the proposed electrodes. The electrical conductivities of the Cu_3P@3DG and 3DG electrodes *via* 4PP configuration with the electrode spacing of 2 mm were calculated to be 1,076 S m^{-1} and 978 S m^{-1}, respectively. Here, the Cu_3P@3DG electrode exhibited better conductivity as compared to the bare 3DG electrode on graphite substrate. This could be due to the metalloid property of Cu_3P nanoparticles, shown in **Supplementary Figure S7**. To boost the kinetics of Cu_3P, Cu_3P@3DG had been elaborately designed, as schematically shown in **Figure 1A**. A systematic loading optimization of Cu_3P on a 3DG matrix had been performed for extracting the best capacitive performance of Cu_3P@3DG electrodes, as shown in **Figures 2C,D**. Here, the area under the CV curve was gradually increasing without any impressive redox peaks under the loading concentration of Cu_3P that varied from 0.3 to 0.91 mg/ml. Optimizing the weight% of Cu_3P in 3DG electrode, the redox probability of Cu_3P on the 3DG matrix had been controlled until 0.91 mg/ml loading. However, increasing the loading concentration to 1.2 mg/ml and above, the redox peaks appeared more prominent at the same potential as bare Cu_3P with increased current density due to the presence of the 3DG matrix. However, after a further increase in the concentration of Cu_3P until 1.5 mg/ml, the prominent redox peaks appeared. This loading concentration of Cu_3P on 3DG-graphite (0.91 mg/ml loading in 1 cm^2 × 1 cm^2) showed the best performance in galvanostatic charge–discharge curves at 5.13A/g current density (**Figure 2D**). For device fabrication as well as to evaluate the stability of the supercapacitor electrodes, the optimum loading concentration of Cu_3P had been fixed to 0.91 mg/ml. The electrochemical CV curves and GCD performance (with different scan rates) of 3DG and bare Cu_3P on graphite substrate are shown in **Supplementary Figure S8**. However, it had been observed that the C_{sp} value of Cu_3P on glassy carbon electrode (234.8 F/g) was slightly higher than that on graphite electrode (224 F/g) at a fixed current density of 1.28 A/g, which might be due to the interfacial interaction of electroactive material with the electrode substrate. The electrochemical analysis using this hybrid structure was carried out to evaluate its applicability toward energy storage devices. The C_{sp} of Cu_3P@3DG electrode was calculated to be 1,095.85, 901.50, 828.48, 778.70, 740.95, 706.66, 675.37, 590.95, 621.63, 597.45, 574.29, 495.97, and 421.65 F/g at the scan rate of 10, 20, 30, 40, 50, 60, 70, 80, 90, 100, 110, 150, and 200 mV/s, respectively from **Figure 2E**. Alternatively, the C_{sp} extracted from the GCD measurements (**Figure 2F**) of the Cu_3P@3DG electrode at various current density were calculated to be 849.81, 771.26, 734.35, 712.35, 692.39, 676.9, 659.98, and 644.75 F/g at 1.28, 2.56, 3.85, 5.13, 6.41, 7.69, 8.97, and 10.268 A/g, respectively (**Supplementary Figure S9**). The nearly isosceles triangular shape of the GCD (**Figure 2F**) implied excellent electron conductivity with tiny voltage drops at different current densities of Cu_3P@3DG electrode. The energy and power density extracted from the charge and discharge analysis were about 118.1, 107.1, 102.0, 99.0, 96.2, 94.1, 91.7, and 89.5 Wh/kg and 641.0, 1,282.0, 1,923.0, 2,564.1, 3,205.2, 3,846.2, 4,487.2, and 7,132.2 W/kg at 1.28, 2.56, 3.85, 5.13, 6.41, 7.69, 8.97, and 10.268 A/g current density, respectively.

The comparative CV curves of the electrodes made of three different electroactive nanomaterials: Cu_3P@3DG, 3DG, and bare Cu_3P were carried at a scan rate of 20 mV/s (**Figure 3A**). The C_{sp} of Cu_3P@3DG, 3DG, and Cu_3P electrodes were calculated to 901.5, 332.7, and 217.7 F/g (from CV curves), respectively, at a scan rate of 20 mV/s. Typically, the electrochemical properties like C_{sp} of Cu_3P@3DG were calculated to be nearly 2.5 times and four times enhanced as compared to bare 3DG and Cu_3P-based electroactive materials, respectively. The results implied that Cu_3P@3DG electrode referred to an excellent EDLC. The GCD measurements of the Cu_3P@3DG, 3DG, and bare Cu_3P on graphide electrodes at fixed current densities were performed with the potential window of 1.0 V (**Figure 3B**). The Cu_3P@3DG exhibited a high C_{sp} of 850 F/g (from GCD analysis) as compared to 3DG and bare Cu_3P of 336 F/g and 224 F/g, respectively, at a current density of 1.28 A/g. Even at a very high current density of 10.27 A/g, the C_{sp} reached up to 645 F/g which was about 76% of the capacitance retention compared to the current density of 1.28 A/g that invariably referred to the excellent stability of our electroactive material hetero-structure (shown in **Figure 2F**). The primary objective to incorporate 3DG along with Cu_3P platelets was to provide high conductive channels for ion and electron transfer in the charging–discharging process leading to the improvement of the overall performance of hybrid electrodes (An et al., 2014). This hybrid structure could effectively minimize the unwanted agglomeration of Cu_3P particles and simultaneously restricted the possibility of restacking of 3DG porous structure and thereby retaining the large surface area (**Supplementary Figure S10**), higher C_{sp}, better rate capability, and overall device stability.

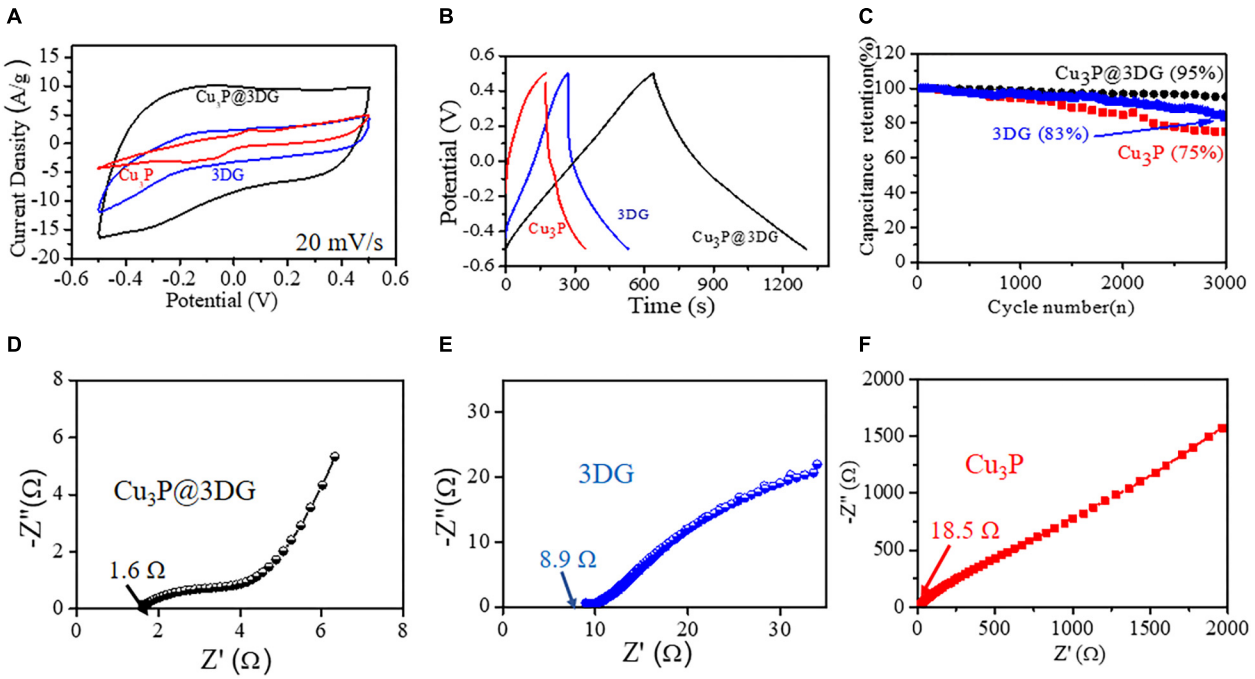

FIGURE 3 | (A) Cyclic voltammetry (CV) curves of the three-dimensional graphene-decorated copper phosphide (Cu_3P@3DG)-graphite (at 0.91 mg/ml), 3DG-graphite, and Cu_3P-graphite at 20 mV/s. **(B)** Galvanostatic charge–discharge curves collected at a fixed current density of 1.28 A/g for Cu_3P@3DG, 3DG, and Cu_3P on graphite electrodes. **(C)** Cycling performance of Cu_3P@3DG, 3DG, and Cu_3P on graphite electrodes at 1.28 A/g current density. **(D–F)** Impedance Nyquist plots of the Cu_3P@3DG, 3DG, and Cu_3P on graphite electrodes, respectively.

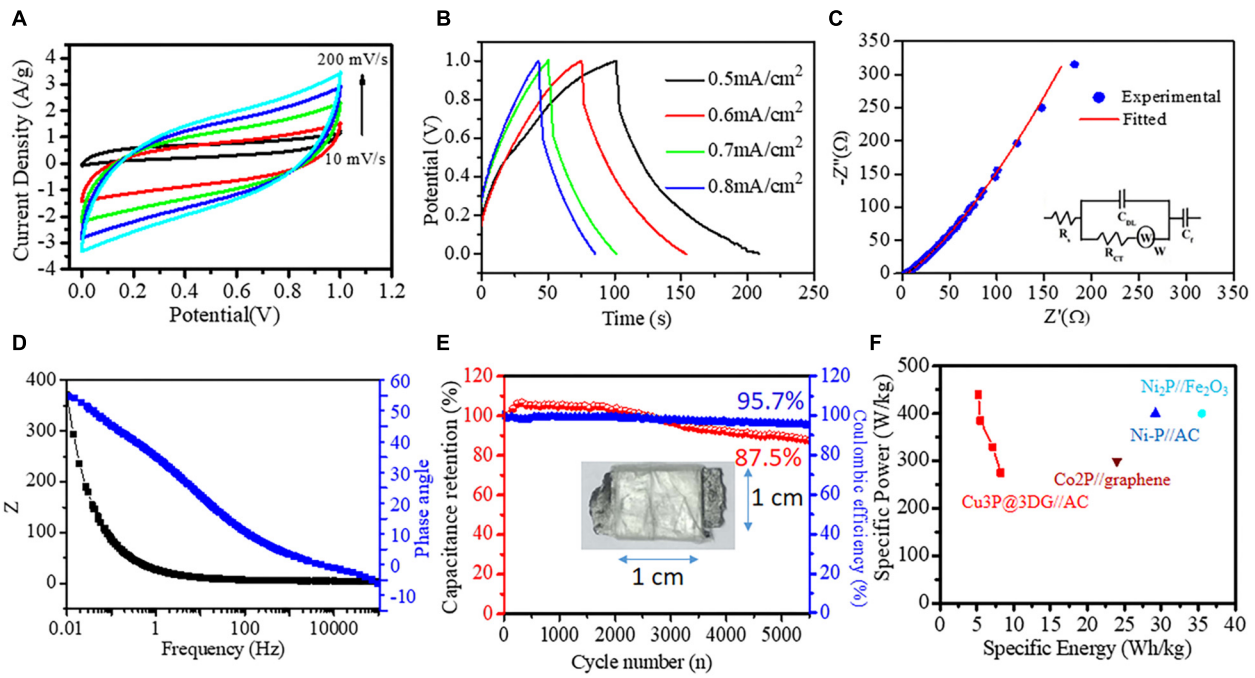

FIGURE 4 | Solid-state asymmetric supercapacitor (ASC). **(A)** Cyclic voltammetry (CV) curves obtained at different scan rates (10, 50, 100, 150, and 200 mV/s). **(B)** Galvanostatic charge–discharge curves obtained at different current densities (0.5, 0.6, 0.7, and 0.8 mA/cm^2). **(C)** Nyquist plot of the asymmetric device with the equivalent circuit as an inset. **(D)** Bode phase angle plot. **(E)** Capacitance retention (red ball-line) and coulombic efficiency (blue ball-line) of the assembled ASC device after 5,500 cycles; ASC device in the inset. **(F)** Ragone plots of ASC devices.

TABLE 1 | Comparison of capacitive performances of this work with those reported in relevant works.

Electrode material	Specific capacitance	Electrolyte	Cyclic stability	ASC device	ASC capacitance	Electrolyte	Energy, Power densities	ASC device stability	References
Ni_2P nanospheres	306.8 F/g at 1A/g	3 M KOH	62.7% retention after 5,000						Wu H. et al., 2016
Ni_2P nanorods	799.2 F/g at 1A/g	3 M KOH	68.4% retention after 5,000						Wu H. et al., 2016
Co_2P nanorods	284 F/g at 1 A/g	3 M KOH							Chen et al., 2016
Ni_2P/GS	1,912 F/g at 5 mA/cm^2	2 M KOH	77.1% retention after 2,300						An et al., 2014
Ni2P/rGO	2,266 F/g at 5 mA/cm^2	2 M KOH							An et al., 2014
Hexagonal copper phosphide (Cu_3P) platelets	224 F/g at 1.28 A/g	1 M Na_2 SO_4	75% retention after 3,000						Present Work
Ni_2P	843.25 F/g at 1 A/g	2 M KOH	96% retention after 1,000	$Ni_2P//Fe_2O_3$	100 F/g at 0.5 A g^{-1}	2 M KOH with one piece of cellulose paper as the separator	35.5 Wh kg^{-1}, 400 W kg^{-1}	96%, 1,000	Wang et al., 2015a
Ni_5P_4	801.5 F/g at 1 A/g	2 M KOH	87% retention after 1,000	$Ni_5P_4//Fe_2O_3$	88.3 F/g at 0.5 A g^{-1}	2 M KOH with one piece of cellulose paper as the separator		86%, 1,000	Wang et al., 2015a
Amorphous Ni-P	964 F/g at 4 A/g	2 M KOH	71.4% retention after 1,000	Ni-P//AC	105 F/g at 5 mV/s	2 mol L^{-1} KOH	29.2 Wh kg^{-1}, 400 W kg^{-1}	84.5% 1,000	Wang et al., 2015b
Co_2P nanoflowers	461 F/g at 1 A/g	6 M KOH		Co_2P//graphene	76.8 F/g at 0.4 A g^{-1}	6 M KOH	24 Wh kg^{-1}, 300 W kg^{-1}	97%, 6,000	Chen et al., 2016
Cu_3P nanotube	177.1 F/g at 3.5 mA/cm^2	1 M H_2SO_4		Cu_3P//CNT	142.8 F/g at 0.75 mA cm^{-2}	0.5 M H_2SO_4	44.6 Wh kg^{-1}, 17,045.7 W kg^{-1}	81.9% 5,000	Chen et al., 2017
Cu_3P@3DG	849.81 F/g at 1.28 A/g	1 M Na_2 SO_4	95% retention after 3,000	Cu_3P@3DG//AC	108.78 F/g at 10 mV/s	PVA KOH gel electrolyte	8.23 Wh kg^{-1}, 439.6 W/kg	82.5%, 5,500	Present Work

However, the bare 3DG (made of three-dimensionally oriented rGO with very low oxygen content shown in **Supplementary Figure S11**) is known to be acting as promising anode materials due to high electronegativity rather than effective cathode material where graphene is difficult to get oxidized under the operating potential window (Hossain et al., 2012). CV analysis of bare glassy carbon and Cu_3P decorated glassy carbon shown in **Supplementary Figure S12**.

The cycle stability had been evaluated for Cu_3P@3DG, 3DG, and hexagonal Cu_3P platelet-based electroactive materials on graphite substrate for its applicability in real phase energy storage devices. **Figure 3C** showed the variation of the C_{sp} retention (%) as a function of the cycle number of the galvanostatic charge–discharge curves of the Cu_3P@3DG, 3DG, and hexagonal Cu_3P platelets at a fixed current density of 1.28 A/g. Surprisingly, after 3,000 cycles, the capacitive retention of Cu_3P@3DG was found to be 95%, whereas that of 3DG was 83%. However, the stability degraded to 75% for bare Cu_3P platelets. This gave us a clear understanding that the 3DG matrix was protecting Cu_3P platelets from chemical degradation as well as agglomeration due to its high electrical and thermal conductivities. These excellent properties of 3DG in our nanohybrid materials had been further evaluated by characteristic electrochemical impedance study. **Figures 3D–F** showed the Nyquist plot of the Cu_3P@3DG, bare 3DG, and Cu_3P electrodes, respectively. In the spectrum, the equivalent series resistances of Cu_3P@3DG, 3DG, and bare Cu_3P on graphite electrodes were calculated to be 1.6, 8.9, and 18.5 **Ω**, respectively, which showed favorable conductivity (evident from the 4PP *I-V* characteristic, shown in **Supplementary Figure S7**) and very low internal resistance of Cu_3P@3DG hybrid for high specific power density.

The asymmetric supercapacitor (ASC) device was fabricated to investigate the potential application of Cu_3P@3DG nanohybrid as a positive electrode and AC as a negative electrode on a graphite substrate. The electrochemical performance of the ASC device was analyzed *via* CV at different scan rates, and GCD measurements were done at various current densities, as shown in **Figures 4A,B**. The potential window of the ASC Cu_3P@3DG and AC electrodes was fixed to be 0–1 V. **Figure 4A** displayed the CV curves of the ASC device at different scan rates with a constant potential window, which showed rectangular like CV curves without redox peaks. It indicated the excellent reversibility and kinetics for electrochemical reactions over the ASC electrode. The C_{sp} of the device was calculated to be 108.78, 61.65, 47.30, 39.86, and 35.09 F/g (217.56, 123.32, 94.61, 79.74, and 70.20 mF/cm^2) at the scan rate of 10, 50, 100, 150, and 200 mV/s respectively. Alternatively, the C_{sp} extracted from the GCD measurements of the device, as shown in **Figure 4B**, at various current densities were calculated to be 59.72, 51.82, 39.53, and 37.53 F/g (107.8, 94.33, 71.96, and 68.32 mF/cm^2) at 0.5, 0.6, 0.7, and 0.8 mA/cm^2 current densities, respectively. The energy and power densities were calculated to be 8.23, 7.2, 5.5, and 5.2 Wh/kg and 274.7, 329.7, 384.6, and 439.6 W/kg at 0.5, 0.6, 0.7, and 0.8 mA/cm^2 current densities, respectively. To further elucidate the origin of high electrochemical performance, the electrochemical impedance spectrum (EIS) was carried out to examine the Cu_3P@3DG//AC supercapacitor device. **Figure 4C** showed the Nyquist plot, the combined resistance Rs (the intrinsic, contact, and electrolyte resistance) of 4.24 **Ω**, the Cdl (the electric double layer capacitance) of 70.4 μF, and the Rct (the resistance of Faradic reaction) of 714 m**Ω**. The inclined line in the low-frequency region represented the Warburg impedance (W) of 19.2 mMho, and constant phase element (C_F) 81.1 mMho. Simultaneously, the apparent straight-line nature of the plot in a low-frequency region described the ideal capacitive behavior of this prototype ASC device. The corresponding equivalent circuit was drawn based on the complex non-linear least-squares fitting method, shown as an inset of **Figure 4C**. **Figure 4D** displayed the Bode phase angle plot of Cu_3P@3DG//AC. The absence of a horizontal segment in the Z-frequency plot at the low-frequency range revealed good charge-transfer behavior. Simultaneously, the high value of the phase angle curve manifested the great capacitive behavior of Cu_3P@3DG//AC at the low-frequency range. Moreover, the long-term cycling stability performance was examined by GCD analysis at a current density of 0.7 mA/cm^2. This supercapacitor device has demonstrated 82.5% capacitance retention after 5,500 cycles exhibiting outstanding cycling stability with 96% coulombic efficiency, as shown in **Figure 4E**. **Figure 4F** displayed the Ragone plot of ASC (Cu_3P@3DG//AC) device. All these observations indicated that the Cu_3P@3DG exhibited good electrochemical performance that could promote it to be an excellent material for its applicability in the next-generation energy storage device. In all the listed combination of metal phosphides, a direct comparison was not possible because of various factors like two-electrode experiment was performed in both solid and liquid state and the concentration and type of elecrolytes were different in all experimental conditions which had a prominent effect on the overall performance of the materials.

Table 1 depicts the transition metal phosphide-based active electrodes that so far had been tested as promising materials for supercapacitor devices. The synthesis of the metal phosphides with optimized nanostructures and composition was a real challenge. Although the reported specific capacitances of the active materials like Ni-P, Ni_2P, CoP, Co_2P, and Cu_3P with different morphologies were quite high, but the working potential and capacitance retention were significantly low. However, it was found to be quite challenging to expand the working potential of the electrodes for practical applications. Here, we offered a strategy to synthesize hexagonal Cu_3P platelets with 3DG as promising electrode materials for supercapacitors *via* controlling the directionality of the growth as well as engineering the facile interface between electrodes to electroactive materials which worked well in negative as well as positive working potentials.

CONCLUSION

In summary, the facile synthesis procedure of hexagonal Cu3P platelets and the fabrication of a heterostructure Cu_3P with interwoven 3DG on graphite electrode (1 cm^2 × 1 cm^2) shows a simple way to design a supercapacitor device for practical applications. The Cu_3P@3DG nanohybrid facilitates electron transfer and promotes kinetics with long cycling stability *via* lowering the internal resistance and providing electrochemical

stability of Cu_3P platelets. The high conductive channels for ions and electron transfer in the charging–discharging process leads to an enhancement of the overall device performance. The specific capacitance of the Cu_3P@3DG is 849.81 F/g at a current density of 1.28 A/g and also exhibits superior cycling performance, with 95% retention of capacitance after 3,000 cycles at a current density of 1.28 A/g. In contrast, the solid-state asymmetric device shows the C_{sp} of 109 F/g (from the CV) and 60 F/g (from GCD) with a capacitive retention of 82.5% and coulombic efficiency of 96% after 5,500 cycles, respectively. Due to the higher capacitance, lower cost, and excellent cycle stability of the Cu_3P@3DG, it is anticipated that the material has potential for next-generation energy storage applications.

DATA AVAILABILITY STATEMENT

All datasets generated for this study are included in the article/**Supplementary Material**.

AUTHOR CONTRIBUTIONS

SBK designed the work. SSK and SA performed the experiments and characterizations. SSK and SR prepared the electrodes assembly of the samples and analyzed the electrochemical data. KG and GN participated in interpreting and analyzing all data and finalized the manuscript. GY and LM helped to characterize HRTEM and TEM analysis. All authors read and approved the final manuscript.

FUNDING

KG is thankful for the financial support from Nano Mission, Department of Science & Technology, India [Grant No: SR/NM/NS-91/2016 (G)]. GN would also like to thank the Israel Science Foundation, VATAT, and the Israel Prime Minister's Office fuel alternative initiative for partial funding of this study under the Israel National Research Center for Electrochemical Propulsion (INREP).

ACKNOWLEDGMENTS

SBK would like to thank the Planning and Budgeting Committee of the Council for Higher Education for his PBC postdoctoral fellowship.

SUPPLEMENTARY MATERIAL

The Supplementary Material for this article can be found online at: https://www.frontiersin.org/articles/10.3389/fmats.2020.00030/full#supplementary-material

REFERENCES

An, C., Wang, Y., Li, L., Qiu, F., Xu, Y., Xu, C., et al. (2014). Effects of highly crumpled graphene nanosheets on the electrochemical performances of pseudocapacitor electrode materials. *Electrochim. Acta* 133, 180–187. doi: 10.1016/j.electacta.2014.04.056

Augustyn, V., Simon, P., and Dunn, B. (2014). Pseudocapacitive oxide materials for high-rate electrochemical energy storage. *Energy Environ. Sci.* 7, 1597–1614. doi: 10.1039/c3ee44164d

Aziz, S. T., and Islam, R. U. (2018). Polymer-supported Cu–nanoparticle as an efficient and recyclable catalyst for oxidative homocoupling of terminal alkynes. *Catal. Lett.* 148, 205–213. doi: 10.1007/s10562-017-2237-8

Barry, B. M., Gillan, E. G., and Mater, R. E. C. (2008). Low-temperature solvothermal synthesis of phosphorus-rich transition-metal phosphides. *Chem. Mater.* 20, 2618–2620. doi: 10.1021/cm703095z

Brock, S. L., Perera, S. C., and Stamm, K. L. (2004). Chemical routes for production of transition-metal phosphides on the nanoscale: implications for advanced magnetic and catalytic materials. *Chem. - A Eur. J.* 10, 3364–3371. doi: 10.1002/chem.200305775

Brock, S. L., and Senevirathne, K. (2008). Recent developments in synthetic approaches to transition metal phosphide nanoparticles for magnetic and catalytic applications. *J. Solid State Chem.* 181, 1552–1559. doi: 10.1016/j.jssc.2008.03.012

Cao, J., Lei, C., Yang, B., Li, Z., Lei, L., Hou, Y., et al. (2019). Zeolitic imidazolate framework-derived core-shell-structured CoS 2 /CoS2 -N-C supported on electrochemically exfoliated graphene foil for efficient oxygen evolution. *Batter. Supercaps* 2, 348–354. doi: 10.1002/batt.201800098

Chen, X., Cheng, M., Chen, D., and Wang, R. (2016). Shape-controlled synthesis of co2p nanostructures and their application in supercapacitors. *ACS Appl. Mater. Interfaces* 8, 3892–3900. doi: 10.1021/acsami.5b10785

Chen, Y., Zhang, W., Zhou, D., Tian, H., Su, D., Wang, C., et al. (2019). Co–Fe mixed metal phosphide nanocubes with highly interconnected-pore architecture as an efficient polysulfide mediator for lithium-sulfur batteries. *ACS Nano* 13, 4731–4741. doi: 10.1021/acsnano.9b01079

Chen, Y. C., Chen, Z. B., Lin, Y. G., and Hsu, Y. K. (2017). Synthesis of copper phosphide nanotube arrays as electrodes for asymmetric supercapacitors. *ACS Sustain. Chem. Eng.* 5, 3863–3870. doi: 10.1021/acssuschemeng.6b03006

Ding, L., Zhang, K., Chen, L., Yu, Z., Zhao, Y., Zhu, G., et al. (2019). Formation of three-dimensional hierarchical pompon-like cobalt phosphide hollow microspheres for asymmetric supercapacitor with improved energy density. *Electrochim. Acta* 299, 62–71. doi: 10.1016/j.electacta.2018.12.180

Fan, M., Chen, Y., Xie, Y., Yang, T., Shen, X., Xu, N., et al. (2016). Half-cell and full-cell applications of highly stable and binder-free sodium-ion batteries based on Cu3P nanowire anodes. *Adv. Funct. Mater.* 26, 5019–5027. doi: 10.1002/adfm.201601323

Han, A., Zhang, H., Yuan, R., Ji, H., and Du, P. (2017). Crystalline copper phosphide nanosheets as an efficient janus catalyst for overall water splitting. *ACS Appl. Mater. Interfaces* 9, 2240–2248. doi: 10.1021/acsami.6b10983

Hao, J., Yang, W., Huang, Z., and Zhang, C. (2016). Superhydrophilic and superaerophobic copper phosphide microsheets for efficient electrocatalytic hydrogen and oxygen evolution. *Adv. Mater. Interfaces* 3:1600236. doi: 10.1002/admi.201600236

Henkes, A. E., Vasquez, Y., and Schaak, R. E. (2007). Converting metals into phosphides: a general strategy for the synthesis of metal phosphide nanocrystals. *J. Am. Chem. Soc.* 129, 1896–1897. doi: 10.1021/ja068502l

Hossain, M. Z., Johns, J. E., Bevan, K. H., Karmel, H. J., Liang, Y. T., Yoshimoto, S., et al. (2012). Chemically homogeneous and thermally reversible oxidation of epitaxial graphene. *Nat. Chem.* 4, 305–309. doi: 10.1038/nchem.1269

Hou, C. C., Chen, Q. Q., Wang, C. J., Liang, F., Lin, Z., Fu, W. F., et al. (2016). Self-supported cedarlike semimetallic Cu3P nanoarrays as a 3D high-performance Janus electrode for both oxygen and hydrogen evolution under basic conditions. *ACS Appl. Mater. Interfaces* 8, 23037–23048. doi: 10.1021/acsami.6b06251

Itzhak, A., Teblum, E., Girshevitz, O., Okashy, S., Turkulets, Y., Burlaka, L., et al. (2018). Digenite (Cu9S5): layered p-type semiconductor grown by reactive

annealing of copper. *Chem. Mater.* 30, 2379–2388. doi: 10.1021/acs.chemmater.8b00191

Jayalakshmi, M., and Balasubramanian, K. (2008). Cyclic voltammetric behavior of copper powder immobilized on paraffin impregnated graphite electrode in dilute alkali solution. *Int. J. Electrochem. Sci.* 3, 1277–1287.

Jin, Y., Zhao, C., Wang, Y., Jiang, Q., Ji, C., and Jia, M. (2017). Large-scale production of Cu3P nanocrystals for ultrahigh-rate supercapacitor. *Ionics* 23, 3249–3254. doi: 10.1007/s11581-017-2267-7

Kumar, S., Aziz, S. T., Girshevitz, O., and Nessim, G. D. (2018). One-step synthesis of N-Doped graphene quantum dots from chitosan as a sole precursor using chemical vapor deposition. *J. Phys. Chem. C* 122, 2343–2349. doi: 10.1021/acs.jpcc.7b05494

Kumar, S., Gonen, S., Friedman, A., Elbaz, L., and Nessim, G. D. (2017). Doping and reduction of graphene oxide using chitosan-derived volatile N-heterocyclic compounds for metal-free oxygen reduction reaction. *Carbon N. Y.* 120, 419–426. doi: 10.1016/j.carbon.2017.05.071

Li, D., Baydoun, H., Verani, C. N., and Brock, S. L. (2016). Efficient water oxidation using CoMnP nanoparticles. *J. Am. Chem. Soc.* 138, 4006–4009. doi: 10.1021/jacs.6b01543

Li, X., Elshahawy, A. M., Guan, C., and John, W. (2017). Metal phosphides and phosphates-based electrodes for electrochemical supercapacitors. *Small* 13:1701530. doi: 10.1002/smll.201701530

Li, Z., Ding, J., and Mitlin, D. (2015). Tin and tin compounds for sodium-ion battery anodes: phase transformations and performance. *Acc. Chem. Res.* 48, 1657–1665. doi: 10.1021/acs.accounts.5b00114

Liang, H., Xia, C., Jiang, Q., Gandi, A. N., Schwingenschlögl, U., and Alshareef, H. N. (2017). Low-temperature synthesis of ternary metal phosphides using plasma for asymmetric supercapacitors. *Nano Energy* 35, 331–340. doi: 10.1016/j.nanoen.2017.04.007

Lin, Y.-G., Hsu, Y.-K., Lin, Y.-C., Chang, Y.-H., Chen, S.-Y., and Chen, Y.-C. (2016). Synthesis of Cu2O nanoparticle films at room temperature for solar water splitting. *J. Colloid Interface Sci.* 471, 76–80. doi: 10.1111/poms.12938

Liu, S., He, X., Zhu, J., Xu, L., and Tong, J. (2016). Cu3P/RGO nanocomposite as a new anode for lithium-ion batteries. *Sci. Rep.* 6, 1–10. doi: 10.1038/srep35189

Liu, S., Li, S., Wang, J., Shi, Q., and Li, M. (2012). Surfactant-assisted synthesis and electrochemical performances of Cu 3 P dendrites. *Mater. Res. Bull.* 47, 3352–3356. doi: 10.1016/j.materresbull.2012.07.026

López-Ortega, A., Lottini, E., Fernández, C. D. J., and Sangregorio, C. (2015). Exploring the magnetic properties of cobalt-ferrite nanoparticles for the development of a rare-earth-free permanent magnet. *Chem. Mater.* 27, 4048–4056. doi: 10.1021/acs.chemmater.5b01034

Mukherjee, D., and Austeria, M. (2016). Two-dimensional, few-layer for electrochemical hydrogen evolution over phosphochalcogenide, FePS3: a new catalyst wide pH range. *ACS Energy Lett.* 1, 367–372. doi: 10.1021/acsenergylett.6b00184

Olofsson, O. (1972). The crystal structure of Cu3P. *Acta Chem. Scand.* 26, 2777–2787. doi: 10.3891/acta.chem.scand.26-2777

Pfeiffer, H., Tancret, F., Bichat, M. P., Monconduit, L., Favier, F., and Brousse, T. (2004). Air stable copper phosphide (Cu3P): a possible negative electrode material for lithium batteries. *Electrochem. Commun.* 6, 263–267. doi: 10.1016/j.elecom.2003.12.012

Pfeiffer, H., Tancret, F., and Brousse, T. (2005). Synthesis, characterization and electrochemical properties of copper phosphide (Cu3P) thick films prepared by solid-state reaction at low temperature: a probable anode for lithium-ion batteries. *Electrochim. Acta* 50, 4763–4770. doi: 10.1016/j.electacta.2005.02.024

Poli, F., Wong, A., Kshetrimayum, J. S., Monconduit, L., and Letellier, M. (2016). In situ NMR insights into the electrochemical reaction of Cu3P electrodes in lithium batteries. *Chem. Mater.* 28, 1787–1793. doi: 10.1021/acs.chemmater.5b04802

Riyajuddin, S. K., Aziz, S. K. T., Kumar, S., Nessim, G. D., and Ghosh, K. (2019). 3D-graphene decorated with g-C_3N_4/Cu_3P composite: a noble metal-free bifunctional electrocatalyst for overall water splitting. *ChemCatChem*. doi: 10.1002/cctc.201902065

Seo, B., Baek, D. S., Sa, Y. J., and Joo, S. H. (2016). Shape effects of nickel phosphide nanocrystals on hydrogen evolution reaction. *CrystEngComm* 18, 6083–6089. doi: 10.1039/c6ce00985a

Shao, Y., Shi, X., and Pan, H. (2017). Electronic, magnetic, and catalytic properties of thermodynamically stable two-dimensional transition-metal phosphides. *Chem. Mater.* 29, 8892–8900. doi: 10.1021/acs.chemmater.7b03832

Singh, K., Kumar, S., Agarwal, K., Soni, K., Ramana Gedela, V., and Ghosh, K. (2017). Three-dimensional graphene with MoS 2 nanohybrid as potential energy storage/transfer device. *Sci. Rep.* 7:9458. doi: 10.1038/s41598-017-09266-2

Sivula, K., and Van De Krol, R. (2016). Semiconducting materials for photoelectrochemical energy conversion. *Nat. Rev. Mater* 1:15010. doi: 10.1038/natrevmats.2015.10

Sun, Z., Yue, Q., Li, J., Xu, J., Zheng, H., and Du, P. (2015). Copper phosphide modified cadmium sulfide nanorods as a novel p-n heterojunction for highly efficient visible-light-driven hydrogen production in water. *J. Mater. Chem. A* 3, 10243–10247. doi: 10.1039/c5ta02105g

Wang, D., Kong, L., Liu, M. C., Luo, Y. C., and Kang, L. (2015a). An approach to preparing Ni-P with different phases for use as supercapacitor electrode materials. *Chem. A Eur. J.* 21, 17897–17903. doi: 10.1002/chem.201502269

Wang, D., Kong, L., Liu, M., Zhang, W., and Luo, Y. (2015b). Amorphous Ni-P materials for high-performance pseudocapacitors. *J. Power Sources* 274, 1107–1113. doi: 10.1016/j.jpowsour.2014.10.179

Wang, X., Li, M., Chang, Z., Wang, Y., Chen, B., Zhang, L., et al. (2015c). Orientated Co 3 O 4 nanocrystals on MWCNTs as superior battery-type positive electrode material for a hybrid capacitor. *J. Electrochem. Soc.* 162, A1966–A1971. doi: 10.1149/2.0041511jes

Wang, J., Yang, Q., Zhang, Z., and Sun, S. (2010). Phase-controlled synthesis of transition-metal phosphide nanowires by ullmann-type reactions. *Chem. A Eur. J.* 16, 7916–7924. doi: 10.1002/chem.200902151

Wang, W., Zhang, L., Xu, G., Song, H., Yang, L., Zhang, C., et al. (2018). Structure-designed synthesis of CoP Microcubes from metal-organic frameworks with enhanced supercapacitor properties. *Inorg. Chem.* 57, 10287–10294. doi: 10.1021/acs.inorgchem.8b01524

Wei, S., Qi, K., Jin, Z., Cao, J., Zheng, W., Chen, H., et al. (2016). One-step synthesis of a self-supported copper phosphide nanobush for overall water splitting. *ACS Omega* 1, 1367–1373. doi: 10.1021/acsomega.6b00366

Wu, H., Ni, Y., Wang, M., and Lu, D. (2016). Shape-controlled synthesis and performance comparison of Ni2P nanostructures. *CrystEngComm* 18, 5155–5163. doi: 10.1039/c6ce00386a

Wu, J., Zhang, Q., Zhou, A., Huang, Z., Bai, H., and Li, L. (2016). Phase-separated polyaniline/graphene composite electrodes for high-rate electrochemical supercapacitors. *Adv. Mater.* 28, 10211–10216. doi: 10.1002/adma.201601153

Xue, S., Chen, L., Liu, Z., Cheng, H., and Ren, W. (2018). NiPS 3 nanosheet - graphene composites as highly efficient electrocatalysts for oxygen evolution reaction. *ACS Nano* 2018, 5297–5305. doi: 10.1021/acsnano.7b09146

Zhang, Y., Wang, G., Wang, L., Tang, L., Zhu, M., Wu, C., et al. (2019). Graphene-encapsulated CuP 2 : a promising anode material with high reversible capacity and superior rate-performance for sodium-ion batteries. *Nano Lett* 196, 2575–2582. doi: 10.1021/acs.nanolett.9b00342

Zhou, K., Zhou, W., Yang, L., Lu, J., Cheng, S., Mai, W., et al. (2015). Ultrahigh-performance pseudocapacitor electrodes based on transition metal phosphide nanosheets array via phosphorization: a general and effective approach. *Adv. Funct. Mater.* 25, 7530–7538. doi: 10.1002/adfm.201503662

Zhu, L., Wu, W., Zhu, Y., Tang, W., and Wu, Y. (2015). Composite of CoOOH nanoplates with multiwalled carbon nanotubes as superior cathode material for supercapacitors. *J. Phys. Chem. C* 119, 7069–7075. doi: 10.1021/acs.jpcc.5b01498

Conflict of Interest: The authors declare that the research was conducted in the absence of any commercial or financial relationships that could be construed as a potential conflict of interest.